ACS Catalysis

Research Article

pubs.acs.org/acscatalysis

Role of Tungsten Doping on the Surface States in $BiVO_4$ Photoanodes for Water Oxidation: Tuning the Electron Trapping Process

Qin Shi,[†,‡] Sebastián Murcia-López,[‡] Pengyi Tang,[‡,§] Cristina Flox,[‡] Joan R. Morante,[‡,∥] Zhaoyong Bian,[⊥] Hui Wang,*[,†] and Teresa Andreu*[,‡]

[†]College of Environmental Science and Engineering, Beijing Forestry University, Beijing 100083, PR China

[‡]Department of Advanced Materials for Energy, Catalonia Institute for Energy Research (IREC), Catalonia, Spain

[§]Catalan Institute of Nanoscience and Nanotechnology (ICN2), CSIC and The Barcelona Institute of Science and Technology (BIST), Campus UAB, Bellaterra, 08193 Barcelona, Spain

[∥]University of Barcelona (UB), Marti i Franquès 1, 08028 Barcelona, Catalonia, Spain

[⊥]College of Water Sciences, Beijing Normal University, Beijing 100875, PR China

Supporting Information

ABSTRACT: The nanostructured $BiVO_4$ photoanodes were prepared by electrospinning and were further characterized by XRD, SEM, and XPS, confirming the bulk and surface modification of the electrodes attained by W addition. The role of surface states (SS) during water oxidation for the as-prepared photoanodes was investigated by using electrochemical, photoelectrochemical, and impedance spectroscopy measurements. An optimum 2% doping is observed in voltammetric measurements with the highest photocurrent density at 1.23 V_{RHE} under back side illumination. It has been found that a high PEC performance requires an optimum ratio of density of surface states (N_{SS}) with respect to the charge donor density (N_d), to give both good conductivity and enough surface reactive sites. The optimum doping (2%) shows the highest N_d and SS concentration, which leads to the high film conductivity and reactive sites. The reason for SS acting as reaction sites (i-SS) is suggested to be the reversible redox process of V^{5+}/V^{4+} in semiconductor bulk to form water oxidation intermediates through the electron trapping process. Otherwise, the irreversible surface reductive reaction of VO_2^+ to VO^{2+} though the electron trapping process raises the surface recombination. W doping does have an effect on the surface properties of the $BiVO_4$ electrode. It can tune the electron trapping process to obtain a high concentration of i-SS and less surface recombination. This work gives a further understanding for the enhancement of PEC performance caused by W doping in the field of charge transfer at the semiconductor/electrolyte interface.

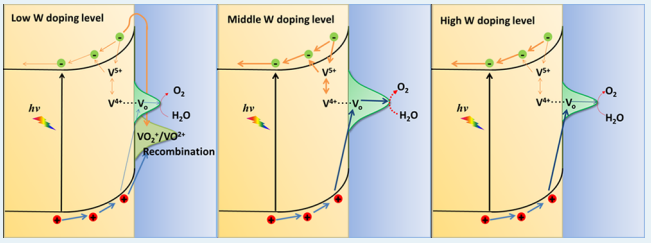

KEYWORDS: *bismuth vanadate, water splitting, photoanode, tungsten doping, surface states*

1. INTRODUCTION

Photoelectrochemical (PEC) water splitting to produce clean hydrogen offers a desirable approach to solving global environmental and energy problems.[1,2] Nonexpensive metal oxide materials such as TiO_2,[3] WO_3,[4] $BiVO_4$,[4] and Fe_2O_3[5,6] have been explored as photoelectrode materials, with inherent stability in aqueous electrolytes, band gap edge alignment that drives force toward water oxidation, and relatively abundant materials. As one of most promising n-type semiconductors, bismuth vanadate with monoclinic structure (ms-$BiVO_4$) has attracted considerable attention, owing to its good performance for various applications, such as photoelectrochemical water splitting and photocatalytic processes including selective oxidation and organic pollutant degradation under visible light illumination.[7−10] However, there are three main limitations in the $BiVO_4$ photoanode: excessive surface recombination, poor charge transport, and sluggish water oxidation kinetics, leading typically to low efficiencies.[7]

Doping $BiVO_4$ is a promising strategy to alleviate its intrinsic limitations. An important number of studies have been devoted to introducing metal atoms (such as Mo and W) to the $BiVO_4$ lattice in order to improve the water oxidation efficiency.[11−14] For instance, Mullins et al. synthesized porous, nanostructured $BiVO_4$ films incorporating Mo and W with a Bi/V/Mo/W atomic ratio of 46:46:6:2 that demonstrated better PEC performance with photocurrent densities 10 times higher than pure $BiVO_4$.[15] In a similar manner, Bard et al. reported a strategy with W- and Mo-doped $BiVO_4$ also showing 10 times improvements in the photocurrent values for water oxidation.[16]

Received: December 13, 2017
Revised: March 9, 2018
Published: March 9, 2018

DOI: 10.1021/acscatal.7b04277
ACS Catal. XXXX, XXX, XXX−XXX

In general, the enhancement of PEC performance is attributed to an increase of charge donor density (N_d) since dopants substitute V sites and serve as electron donors. According to density functional theory (DFT) calculations, Mo- and W-doping under oxygen-poor growth conditions can produce excellent n-type conductivity.[17] In addition, the effect of the dopant on $BiVO_4$ expresses itself in many ways, including promoting the interfacial and bulk charge separation,[18] removing the hole traps in $BiVO_4$,[19] enhancing hole diffusion length,[12] creating local electric field,[20] decreasing the width of the space charge layer, raising the Fermi level, affecting the morphology, and so on. However, it has been found that an inapposite doping level would raise many unpredictable issues and lead to a decrease PEC performance. For example, the excessive amount of phosphate dopants may become defect sites in $BiVO_4$, which act as electron−hole recombination sites,[20] and W doping has found to strongly decrease the carrier mobility by introducing intermediate-depth donor defects as carrier traps.[21]

It is commonly accepted that surface states (SS) play an important role in photoelectrochemical water oxidation. The SS have been reported to influence charge transfer at the semiconductor/electrolyte interface (SEI) because they can work as reaction sites (i-SS) and/or recombination centers (r-SS) on the electrode surface.[22] Previous studies focus on revealing the SS formation on the photoelectrode during the PEC experiment, tuning SS via various modifications, and determining which intermediates might act as SS. Hamann et al. already investigated the SS on hematite photoanodes. They suggested that the hole trapping process into SS is the first step in the water oxidation process, specifically the reversible oxidation of surface hydroxide species, and water oxidation would proceed only after a buildup of the oxidized intermediates.[23] In addition, they provided direct evidence of high-valent iron-oxo intermediates as the product of the first hole-transfer reaction on the hematite surface using infrared spectroscopy under PEC water-oxidation conditions.[24] $CuWO_4$ also presents a capacitive feature related to SS as the buildup of water oxidation intermediate species on the surface.[25] Furthermore, it has been reported that the SS can be tuned by various modifications to improve the PEC performance. For example, Monllor-Satoca et al. tuned the SS by optimizing titanium doping level on a hematite photoanode to obtain a good balance between the film conductivity and charge transfer reactive sites, resulting in an isoenergetic hole transfer to water mediated by SS.[5] Bottom-up interfacial engineering was reported to tune the SS in hematite multilayer nanowires, which were finely regulated via the atomic addition of an Fe_2TiO_5 layer and FeNiOOH nanodots.[6] Other efforts have been devoted to removing the SS acting as r-SS in hematite; for instance, high temperature treatment (800 °C) and ultrathin Al_2O_3 coating have been used to selectively remove the r-SS.[26,27]

To date, few researchers have reported the presence of SS in $BiVO_4$ photoanodes. Smith et al. first investigated the formation of highly active water oxidation intermediates and/or changes in the chemistry of the surface of $BiVO_4$.[9] Nevertheless, to the best of our knowledge, research focused on the role of tungsten doping on the SS is almost vacant, despite being widely accepted as an alternative for enhancing the performance of $BiVO_4$ photoanodes. In this work, we aim to investigate the SS behavior in W doped $BiVO_4$ photoanodes for PEC water oxidation and give a further understanding into the PEC enhancement attained by doping.

2. EXPERIMENTAL SECTION

2.1. Synthesis of Pristine/W-Doped $BiVO_4$ Photoanodes by Electrospinning. Nanoporous pristine/W-doped $BiVO_4$ photoanodes were prepared by reported electrospinning technology with some modifications in an Yflow Electrospinning equipment.[12] In a typical synthesis procedure, 0.6950 g of bismuth acetate ($C_6H_9BiO_6$) was added into a mixture of 3 mL of acetic acid, 3.75 mL of absolute ethanol, and 3.75 mL of N,N-dimethylformamide (DMF), as a solvent to form a homogeneous solution, followed by the addition of 0.4772 g of $VO(ACAC)_2$ and 1.2 g of polyvinylpyrrolidone (PVP, Mw = 1 300 000). Subsequently, the mixture was magnetically stirred at 80 °C for 2 h and then stirred at room temperature overnight. Then, the precursors were transferred into a 20 mL syringe with a stainless steel needle and then were ejected from the needle to a ground aluminum foil vertically placed at 20 cm with a speed of 0.8 mL h^{-1}. The electrospinning proceeded under high voltage (16 kV), and the fibers were collected after 30 min, on previously washed glasses with fluorine doped tin oxide (FTO, 1 × 1 cm^2), followed by heat treatment. The samples were dried at 80 °C for 1 h and then heated to 500 °C during 1 h with a temperature ramp of 4 °C min^{-1}. The W doped samples were prepared by adding different amounts of W to replace the equivalent weight of $VO(ACAC)_2$: the amounts of W precursors (90 μL, 180 and 450 μL) were introduced to reach 1, 2, and 5% atomic substitution of V. The W precursor was prepared by dissolving 0.9994 g of H_2WO_4 into a mixture of 12 mL of H_2O_2 and 8 mL of H_2O.

2.2. Characterization Techniques. Structure analysis with X-ray diffraction (XRD) was performed by using a Bruker D8 Advance diffractometer equipped with a Cu Kα radiation (0.15417 nm) source, a LYNXEYE super speed detector, and a Ni filter. The morphology of the samples was analyzed by using a Zeiss Auriga field emission scanning electron microscope (FESEM). A PHI 5500 Multitechnique model with Al Kα radiation (1486.6 eV) was used to perform X-ray photoelectron spectroscopy (XPS) measurements. Optical properties of all electrodes were recorded in a Lambda 950 UV−vis−NIR spectrometer (PerkinElmer) equipped with a 150 mm integrating sphere coated with Spectralon as a reflectance (white) standard.

2.3. Photoelectrochemical and Electrochemical Measurements. All the photoelectrochemical and electrochemical measurements were conducted in a computer-controlled potentiostat (VMP3, BioLogic Science Instruments) with an undivided three-electrode cell. The counter electrode, reference electrode, and working electrodes were a Pt wire, an Ag/AgCl (3 M KCl) electrode, and the prepared pristine/W-doped $BiVO_4$ electrodes (1 cm^2 geometric area), respectively. A 0.1 M Na_2SO_4 solution (pH = 6.8) was used as an electrolyte. Before the experiments, the electrolyte was purged with N_2 for 30 min. Potentials were converted and reported with respect to the reversible hydrogen electrode (RHE): E (vs RHE) = E (vs Ag/AgCl) + 0.0592 × pH + 0.203. Measurements under illumination were performed using a 150 W AM 1.5G solar simulator (Solar Light Co., 16S-300-002 v 4.0) with an incident light intensity set at 1 Sun (100 mW cm^{-2}). The photoelectrochemical impedance spectroscopy (PEIS) measurements were carried out at different applied biases with an alternate

DOI: 10.1021/acscatal.7b04277
ACS Catal. XXXX, XXX, XXX−XXX

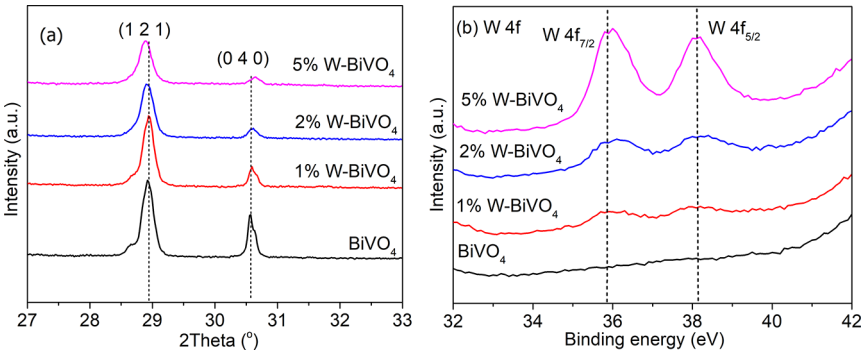

Figure 1. XRD patterns (27−33° region) (a) and W 4f high resolution XPS spectra (b) of pristine and W-doped $BiVO_4$ photoanodes.

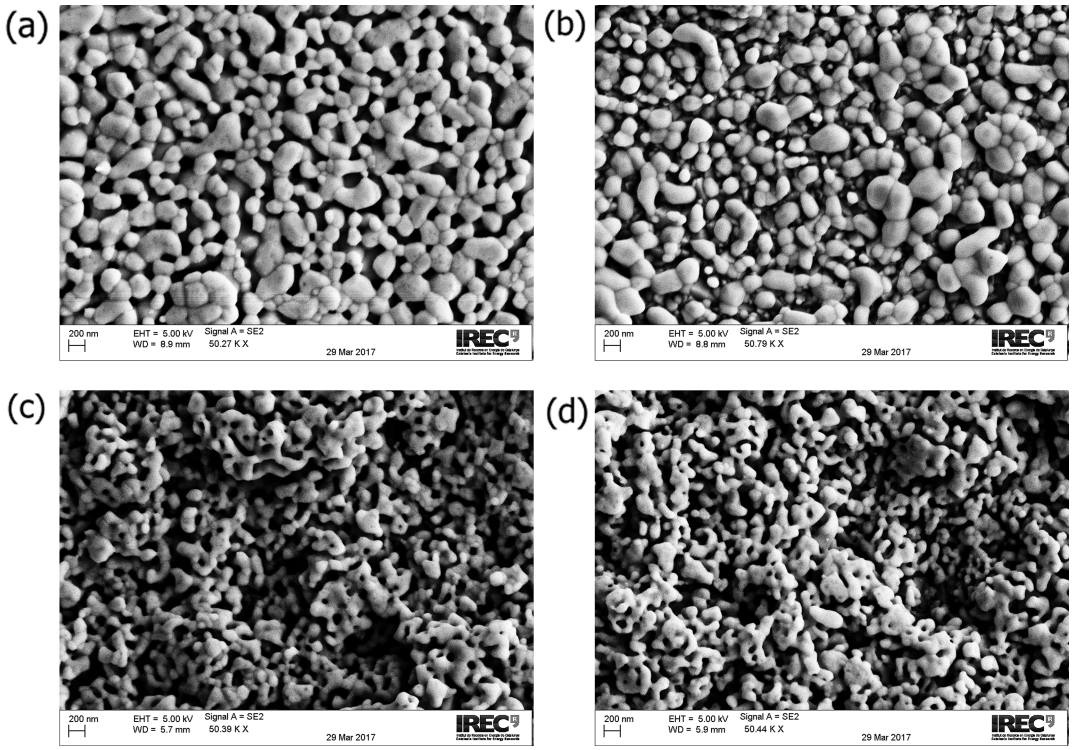

Figure 2. SEM images of $BiVO_4$ (a), 1% W-$BiVO_4$ (b), 2% W-$BiVO_4$ (c), and 5% W-$BiVO_4$ (d) electrodes.

current (AC) perturbation of 25 mV in amplitude and a frequency range from 100 mHz to 1 MHz, both in the dark and under illumination. The numerical fitting of the impedance data was carried out using the Z-fit (BioLogic Associates) corresponding equivalent circuits.

3. RESULTS AND DISCUSSION

3.1. Characterizations of Pristine/W-Doped $BiVO_4$ Photoanodes. XRD measurements were performed on pristine and W-doped $BiVO_4$ photoanodes prepared by electrospinning. As shown in Figure S1, XRD patterns of all photoanodes are consistent with the monoclinic scheelite crystal structure of $BiVO_4$ (JCPDS 014-0688). There is no evidence of any other impurities except for the additional peaks that can be assigned to the SnO_2 (FTO). However, a slight peak shift can be observed in 2% W-$BiVO_4$ and 5% W-$BiVO_4$, as shown in the XRD patterns with a smaller angle range (Figure 1a). The predominant (121) peak at about 28.5° shifts toward the opposite direction of the (040) peak when the W dopant content is higher than 2%, suggesting W is entering into the $BiVO_4$ lattice. However, the fact of the 1% W-$BiVO_4$ sample showing no shift may be attributed to the low W doping level. Further, the surface W element composition was characterized by XPS. As can be seen in Figure 1b, two characteristic peaks located at about 35.8 and 38.2 eV arising from W $4f_{7/2}$ and W $4f_{5/2}$ signals can be observed in the W-doped $BiVO_4$, suggesting W is in a fully oxidized state (W^{6+}) to substitute V^{5+} atoms on the surface of the $BiVO_4$ photoanode, and thus, the positive charge will be compensated by free electrons, increasing its conductivity.[28,29] The peak intensity of W 4f increases by increasing the amount of W dopant. The XRD and XPS results suggest that the bulk and surface of the electrodes have been modified by the addition of W dopant.

Figure 2 shows the morphological characteristics of representative $BiVO_4$ and W-doped $BiVO_4$ photoanodes used for PEC measurements. $BiVO_4$ films are formed of roundish particles with different sizes. Low level incorporation of tungsten (1%) does not change the film morphology (Figure 2b), although slightly smaller feature sizes are observed. However, doping with a higher level of tungsten (2% and

DOI: 10.1021/acscatal.7b04277
ACS Catal. XXXX, XXX, XXX−XXX

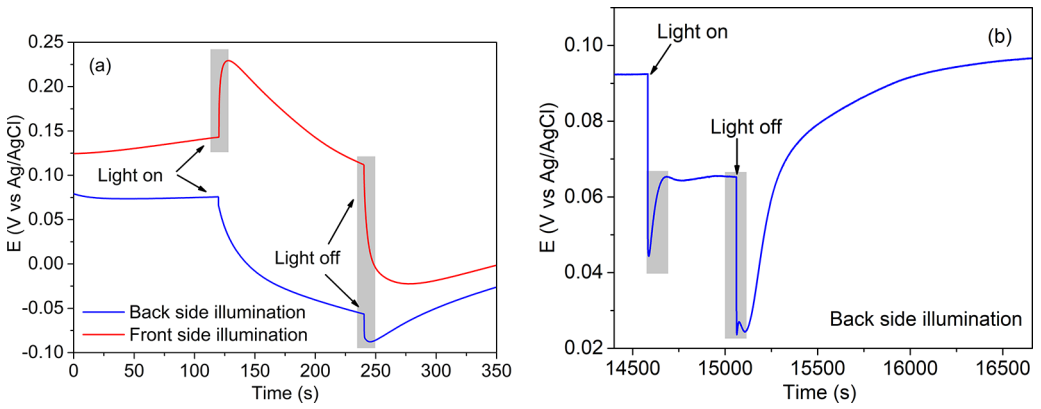

Figure 3. Chronopotentiometric measurement at open-circuit conditions in the dark and under illumination for the $BiVO_4$ electrode with a short stabilization time (a) and after 4 h of stabilization in the dark (b).

5%) does have a remarkable influence on the morphology of the surface. The 2% and 5% W-$BiVO_4$ films have a highly interconnected geometry with an observed smaller diameter so that they present a more porous surface. In addition, absorptance and Tauc plots of $BiVO_4$ and W-doped $BiVO_4$ electrodes are presented in Figure S2. Regardless of the amount of W incorporation, the electrodes have a band gap of approximately 2.5 eV, in line with other techniques, indicating that W incorporation does not alter the band gap of $BiVO_4$.[15,16]

3.2. The Effects of W Doping on Photoelectrochemical Performance for Water Splitting. The PEC performances of all photoanodes were measured by using linear sweep voltammetry (LSV) under both back and front side illumination (Figure S3). Results show that the current density at 1.23 V vs RHE (V_{RHE}) increases first and then decreases as the percentage of W is increased. The intermediate W doping (2% W-$BiVO_4$) leads to the highest photocurrent. Consistent with previous studies, back side illumination may give higher values than the front side illumination in materials with low carrier mobility, since the photogenerated electron has to travel shorter distances between the bulk and FTO.[12] It is worth noting that apparently a larger surface area is present in the W doped $BiVO_4$ electrodes from the observation on SEM (Figure 2). The highly textured surface and porosity would improve hole collection, which is related to the i-SS.[30] As for this, the electrochemically active surface area for each electrode is estimated from the electrochemical double-layer capacitance of the catalytic surface.[31−33] The detailed calculation is shown in the Supporting Information (Figure S4). It is found that only small improvements happen in the roughness factors after W incorporation, indicating the electrochemically active surface area does not significantly increase. Therefore, the slightly larger surface area of W doped $BiVO_4$ electrodes is suggested not to be the main reason for the enhancement of the photoelectrochemical performance in this case. W doping yields a positive shift in the onset potential relative to the parent $BiVO_4$ photoanode under back side illumination (up to 100 mV for 2 and 5% W-$BiVO_4$), while no significant changes in the onset potential are observed when illuminating through the front side. To determine the underlying cause for this different behavior, the open-circuit photovoltage (V_{oc}) measurements were carried out under both side illuminations for $BiVO_4$ (Figure 3a). Note that, for the front side illumination, the $BiVO_4$ photoanode shows a short-lived decay of V_{oc} as soon as the light is on, and an accelerated buildup of V_{oc} in a short time upon shutting down the light (gray area in Figure 3). The same experiment was performed after the $BiVO_4$ electrode was stabilized in the electrolyte in the dark for 4 h (Figure 3b). It can be observed that the same phenomenon happens on a longer time scale, although the short-lived decay of V_{oc} cannot be found under back side illumination in Figure 3a, indicating that the phenomenon does not originate from the absorption of ions when the electrode is just put in the electrolyte. As we know, under open-circuit conditions, the decay and buildup of V_{oc} are attributed to the dissipation and accumulation of photoexcitation electrons in the $BiVO_4$ photoanode.[12,34] In general, the excited electrons accumulate at the semiconductor upon turning the light on, resulting in a shift in the Fermi levels to a more negative potential and hence increasing the V_{oc} until reaching a maximum at the steady state; when illumination is stopped, the accumulated electrons undergo recombination, leading a decay of V_{oc}.[12] We attribute the momentary decay of V_{oc} to a trap of electrons leading to electron "loss" in the electrode bulk at the moment of turning the light on, and the buildup of V_{oc} to a detrapping of electrons leading to electron accumulation in the electrode bulk when the light is off. Interestingly, the momentary decay and buildup of V_{oc} for the back illumination are enhanced after 4 h of stabilization in the dark (Figure 3b). A $BiVO_4$ electrode placed in electrolytes for 4 h should reach a saturation of adsorption for many species in the electrolyte (such as H_2O molecules and OH^-). It is suggested that the adsorption of ions or molecules in electrolytes would be in favor of the trapping or detrapping processes, thus resulting in enhanced momentary decay and buildup of V_{oc}. In addition, these phenomena are also more pronounced when illuminating from the front side of the $BiVO_4$ electrode (Figure 3a). Actually, trap states (such as SS) have been widely investigated in photoelectrochemical water splitting and are attributed to charging or filling of electrons from the conduction band to the SS.[3,6,9,24,35] For example, Gromboni et al. reported suppression on the back-reaction with oxygen in the aqueous phase (recombination) at trap states by coating Al_2O_3 on $BiVO_4$.[36] The presence of SS on the surface of the $BiVO_4$ photoanode is suggested in this case. Figure S5 shows a scheme to illustrate the proposed SS behavior. Under irradiation, the photogenerated electrons are trapped to charge the SS leaving holes in the electrode bulk, thereby resulting in the momentary decay of V_{oc} since SS are promptly full of charge. When the illumination ceases, the "discharging" behavior of SS arises, leading to a momentary accelerated V_{oc} buildup since the released electrons flow to the FTO.

DOI: 10.1021/acscatal.7b04277
ACS Catal. XXXX, XXX, XXX−XXX

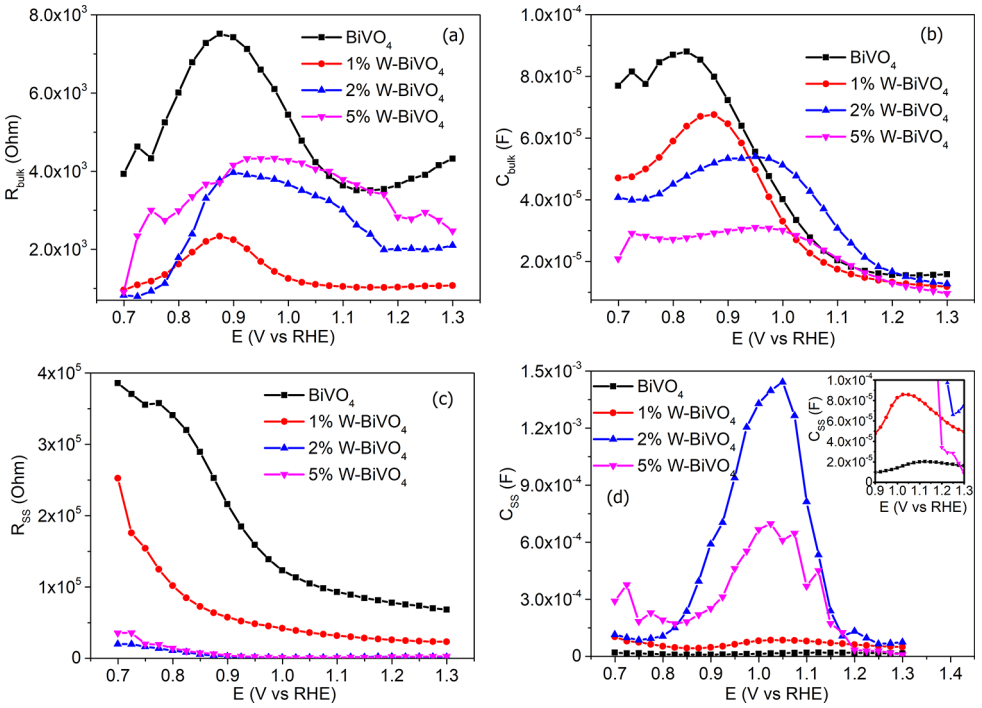

Figure 4. Equivalent circuit parameters obtained from fitting PEIS data for the $BiVO_4$ and 1%, 2%, and 5% W-$BiVO_4$ electrodes under back side illumination. R_{bulk} (a), C_{bulk} (b), R_{SS} (c), and C_{SS} (d) variation as a function of applied potential.

In an effort to find the correlation between W doping treatment and charge transfer behavior, PEIS measurements were performed for the bare $BiVO_4$ electrode as well as the electrodes modified with W. An equivalent circuit (EC) for impedance modeling requires electric elements for all charge transfer resistances in the bulk and SS at SEI. Consequently, the EC shown in Figure S6a is used to fit the impedance spectroscopy data, which has been adopted extensively for n-type semiconductor photoanodes when SS are present.[25,37−39] Nyquist plots resulting from measurements under illumination at 0.7−1.3 V_{RHE} are displayed in Figure S7. It is evident that the fitted results match with the experimental data by comparing the continuous lines and the corresponding markers. Figure 4a shows the charge transfer resistance in bulk (R_{bulk}) associated with charge trapping at surface states as a function of applied potentials. Upon doping the W element into $BiVO_4$, a lower R_{bulk} is achieved, suggesting that the W doping employed herein improves the charge transfer in the bulk. At the 0.8−1.3 V_{RHE} potential window, the R_{bulk} values of all the electrodes are within the same order of magnitude, and the lowest R_{bulk} appears in the 1% W-$BiVO_4$ electrode as compared to the 2% and 5% W-$BiVO_4$ electrodes. As the dopant level is increased, additional impurities might be formed (such as WO_3), as in the case of the 2 and 5% W-$BiVO_4$ electrodes. The formation of deleterious $BiVO_4$−WO_3 heterojunctions (or the increased amount of defects) can also increase the R_{bulk} and give rise to the bulk recombination. Interestingly, capacitance associated with charge accumulation in the bulk (C_{bulk}) shows a peak at 0.7−1.2 V_{RHE} (Figure 4b). This behavior has been attributed to charge accumulation for the redox process of V^{4+}/V^{5+} in the bulk, as reported by Smith et al.[9] The peak potential clearly moves to more positive values, while the peak intensity decreases by increasing the W content. This is consistent with the reduction peak of V^{5+} to V^{4+} at the same potential window in the cyclic voltammetry (CV) measurements shown in Figure S8, indicating that the reductive process of V^{5+} to V^{4+} in bulk tends to be more difficult with increasing the W doping. Therefore, the order of ease to reduce V^{5+} to V^{4+} is 5% W-$BiVO_4$ < 2% W-$BiVO_4$ < 1% W-$BiVO_4$ < $BiVO_4$. According to the DFT calculation by Bard et al., V^{5+} is substituted by W^{6+}, resulting in more V^{4+} both in bulk and at the surface,[16] thus suppressing the V^{5+} to V^{4+} reaction.

Besides the above, it can be observed in Figure 4c that R_{SS}, which is the charge transfer resistance associated with the charge transfer process from surface states, decreases gradually for all the electrodes as the applied potential increases, leading to an increment of associated photocurrent response. The W-doped $BiVO_4$ electrodes show a remarkable reduction of R_{SS}, suggesting W doping does have an effect on the surface properties of $BiVO_4$ in favor of the charge transfer at SEI. Both 2% and 5% W-$BiVO_4$ electrodes give similar and fairly low values of R_{SS} for all shown potentials. Notably, the 2% W-$BiVO_4$ electrode possess a relative minimum R_{SS} at 1.23 V_{RHE} which is about 36-fold lower than that of the pristine $BiVO_4$ electrode. On the other hand, from Figure 4d, we note that the value of the capacitances of SS (C_{SS}) associated with charge accumulation at SEI, exhibiting a typical Gaussian distribution following an ascending order as $BiVO_4$ < 1% W-$BiVO_4$ < 5% W-$BiVO_4$ < 2% W-$BiVO_4$ electrodes. This is attributed to the formation of intermediates which work as reaction sites on the electrode surface in the PEC water oxidation reaction.[9] A low and a large value of R_{SS} and C_{SS}, respectively, would eventually render larger photocurrents.[37] The LSV results (Figure S3) obtained for the doping level in the 2% W-$BiVO_4$ electrode agree with its lowest R_{SS} and highest C_{SS}.

Furthermore, a deeper investigation of interfacial charge transfer process is required to highlight the role of SS. First, to ascertain the percentage of charge that is transferred for different electrodes, the charge proportion at SEI can be estimated through eq 1:[5,6,40]

DOI: 10.1021/acscatal.7b04277
ACS Catal. XXXX, XXX, XXX−XXX

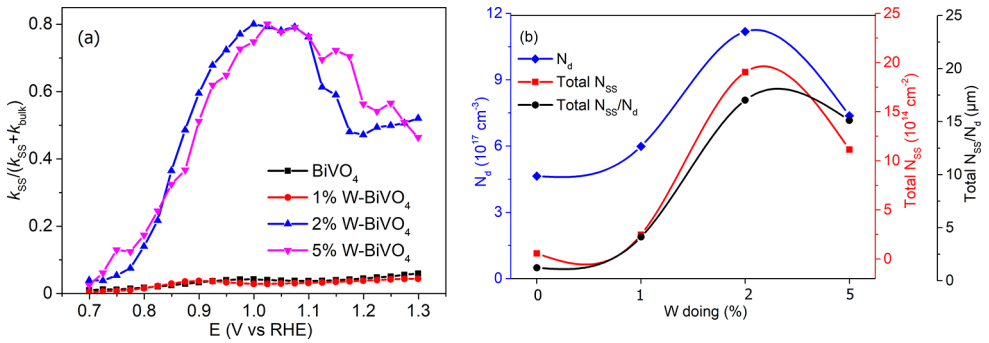

Figure 5. k_{SS} and k_{bulk} ratios at different potentials (a) and total N_{SS}, N_d, and N_{SS}/N_d ratios of the pristine and W-doped $BiVO_4$ electrodes (b).

$$k_{SS}/(k_{bulk} + k_{SS}) = 1/(1 + R_{SS}/R_{bulk}) \quad (1)$$

where k_{bulk} and k_{SS} are the charge transfer rate constants in the bulk and SS, respectively. The values of charge transfer resistances are obtained from the fitting PEIS data shown in Figure 4. The resulting ratios as a function of the potential are shown in Figure 5a. The lower the R_{SS} and larger the R_{bulk} values, the larger the proportion of charge transferred to water at the SEI.[5] Therefore, $BiVO_4$ and 1% W-$BiVO_4$ present the same trend of transfer efficiency and fairly low values of charge transfer ratio in all the applied potentials. It means that few charges would be transferred to the electrolyte with these two electrodes since they suffer significant surface electron−hole recombination. In contrast, the surface recombination in the 2% and 5% W-$BiVO_4$ electrodes has been suppressed leading to remarkable enhancement of charge transfer efficiency, close to 80% at around 1 V_{RHE}. Further, the values of the density of states of SS (N_{SS}) are derived from the fitted capacitances (C_{SS}) as shown in Figure S9. We note that the maximum charge transfer ratio (around 80%) lies in a potential closer to the SS distribution center in line with the statement that the SS can work as reaction sites to provide charge transfer at SEI. The observed tendency is that N_{SS} increases as the percentage of W is increased from 0 to 2% and then decreases again at higher percentages, like the photocurrent (Figure S3) and C_{SS} (Figure 4d), but does not fully agree with the charge transfer ratio at higher potentials. For example, the 5% W-$BiVO_4$ electrode presents higher charge transfer efficiency at SEI than 2% W-$BiVO_4$ at the 1.125−1.25 V_{RHE} potential window.

For this reason, the density of donors (N_d), related to the film conductivity, should be considered. Impedance measurements were performed in the dark to derive the corresponding Mott−Schottky plots. Figure 5b shows a comparison of the total N_{SS}, N_d, and N_{SS}/N_d ratio. The detailed calculation of these parameters is shown in the Supporting Information (Figure S10 and Table S1). The 2% W-$BiVO_4$ electrode displays a higher value of N_d (1.12×10^{18} cm^{-3}) than the pristine $BiVO_4$ (4.64×10^{17} cm^{-3}) and 1% W-$BiVO_4$ (6.00×10^{17} cm^{-3}) electrodes, since the substitutional W atoms on V sites increase the concentration of majority charge carriers.[16] However, N_d decreases with further increasing the W doping level (5%), perhaps because of the formation of a few dopant impurities (such as WO_3), leading to incomplete doping. The total N_{SS}/N_d ratios of the four photoanodes follow the order $BiVO_4$ < 1% W-$BiVO_4$ < 5% W-$BiVO_4$ < 2% W-$BiVO_4$, in line with the PEC performance (Figure S3). The 1% W-$BiVO_4$ and $BiVO_4$ electrodes display low N_{SS}/N_d ratios attributed to presenting a low concentration of N_d, which is not high enough to provide good film conductivity; then the fast bulk/surface recombination results in low N_{SS}. The 5% W-$BiVO_4$ sample shows a remarkable higher total N_{SS}/N_d ratio in comparison with 1% W-$BiVO_4$ mainly because of its high N_{SS} concentration, suggesting that the SS increasing can improve the PEC performance. Notably, the total N_{SS}/N_d ratio of 2% W-$BiVO_4$ is similar to that of 5% W-$BiVO_4$ in agreement with their charge transfer behaviors (Figure 5a). However, 2% W-$BiVO_4$ also exhibits the maximum values in total N_{SS} and N_d. It has been suggested that a high PEC performance requires not only a large N_{SS}/N_d ratio but also numerous total N_{SS} and N_d, to give both good conductivity and enough surface reactive sites.

3.3. Electron Trapping Process for Surface Charge Transfer Site (i-SS). To further understand the charge transfer at the SEI, we performed CV measurements with the $BiVO_4$ electrode in the dark and under illumination (Figure 6). A pair

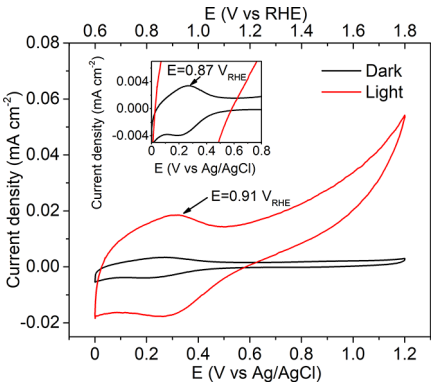

Figure 6. Cyclic voltammograms for $BiVO_4$ under dark and illumination conditions with a 100 mV s^{-1} scan rate.

of reversible anodic and cathodic peaks at about 0.87 V_{RHE} in the dark can be noted, which correspond to the reduction and reoxidation of the V^{5+}/V^{4+} redox system in the $BiVO_4$ bulk (according to eqs 2 and 3).[9,36] A simplified scheme can be found in Figure S11.

$$V^{5+}(bulk) + H^+(aq) + e^-_{inject} \rightarrow V^{4+}(bulk) + H^+(bulk) \quad (2)$$

$$V^{4+}(bulk) + H^+(bulk) \rightarrow V^{5+}(bulk) + H^+(aq) + e^-_{release} \quad (3)$$

It is noteworthy that this redox process is significantly enhanced under illumination. In order to get a better understanding, CV measurements at various scan rates (v) in the dark and under illumination were carried out (Figure 7). A

DOI: 10.1021/acscatal.7b04277
ACS Catal. XXXX, XXX, XXX−XXX

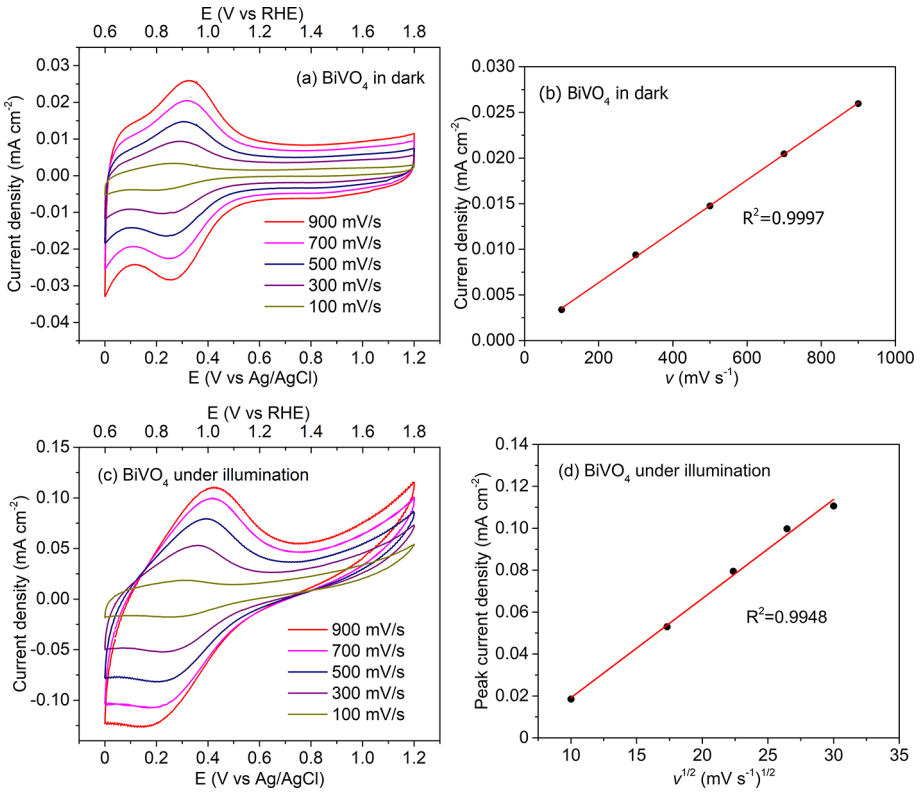

Figure 7. Cyclic voltammograms for $BiVO_4$ at various scan rates (v) in the dark (a) and the corresponding linear relationship between oxidative peak current and v (b). Cyclic voltammograms with $BiVO_4$ at various scan rates (v) under illumination (c) and the corresponding linear relationship between oxidative peak current and $v^{1/2}$ (d).

good liner relationship is observed between the oxidative peak current density and v in the dark (Figure 7a and b), suggesting that the reversible redox process of V^{4+}/V^{5+} in $BiVO_4$ is a surface catalytic reaction in the dark, which means that the reaction rate depends on the number of the active sites (V^{4+} and V^{5+}).[41] A similar behavior is observed in the W-doped $BiVO_4$ electrodes (Figure S12). However, under illumination, the CV curves of $BiVO_4$ show good linear correlation between the oxidative peak current density and $v^{1/2}$ (Figure 7c and d), implying that the reaction turns into a diffusion control reaction.[42,43] The origin of this situation can be that a great amount of reactive sites (V^{4+} and V^{5+}) are produced benefitting from photogenerated electrons. We attribute this to a photoelectron trapping/detrapping process (eqs 4 and 5).

$$\text{Trapping: } V^{5+}(\text{bulk}) + H^{+}(\text{aq}) + e^{-}_{\text{photo}} \rightarrow V^{4+}(\text{bulk}) + H^{+}(\text{bulk}) \quad (4)$$

$$\text{Detrapping: } V^{4+}(\text{bulk}) + H^{+}(\text{bulk}) \rightarrow V^{5+}(\text{bulk}) + H^{+}(\text{aq}) + e^{-}_{\text{photo}} \quad (5)$$

Importantly, the intrinsic reversible behavior observed in the cathodic and anodic directions implies that the trapping and detrapping are fast, so that the traps are not going to act as recombination centers.[35] In contrast, the presence of intermediate V^{4+} formed by the trapping process (eq 4) can induce oxygen vacancies (V_o) on the surface of nanoparticles.[9,44] Some negative charged species tend to be adsorbed on the electrode surface by positive charged V_o.[44] According to the first-principles calculations by Hu et al., when V_o's are present on the surface, the adsorption energies of H_2O_{ads}, OH_{ads}, and O_{ads} are higher, implying enhanced hole transfer from the photoanode surface to the electrolyte.[45] We attribute i-SS to the formation of V_o by the electron trapping process (eq 4) to adsorb oxy/hydroxyl species on the surface of $BiVO_4$, similar to the report by Smith et al.[9] A model is proposed to illustrate the electron trapping/detrapping process under illumination with a formation of i-SS, as shown in Figure S13. The hole can be trapped by V_o and transferred to the electrolyte, as shown in eq 6 and illustrated in Figure S14.

$$V^{4+}(h_{\text{trap}})\cdots OH^{-} \rightarrow V^{4+} + OH^{\bullet} \quad (6)$$

3.4. Electron Trapping Process for Surface Recombination (r-SS).

Figure 8 shows CV curves of $BiVO_4$ in a larger potential range. The resulting curves in the dark and under

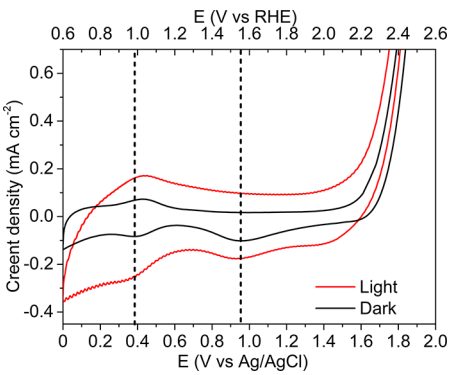

Figure 8. Cyclic voltammograms for $BiVO_4$ under dark and illumination conditions with a 2000 mV s^{-1} scan rate.

DOI: 10.1021/acscatal.7b04277
ACS Catal. XXXX, XXX, XXX−XXX

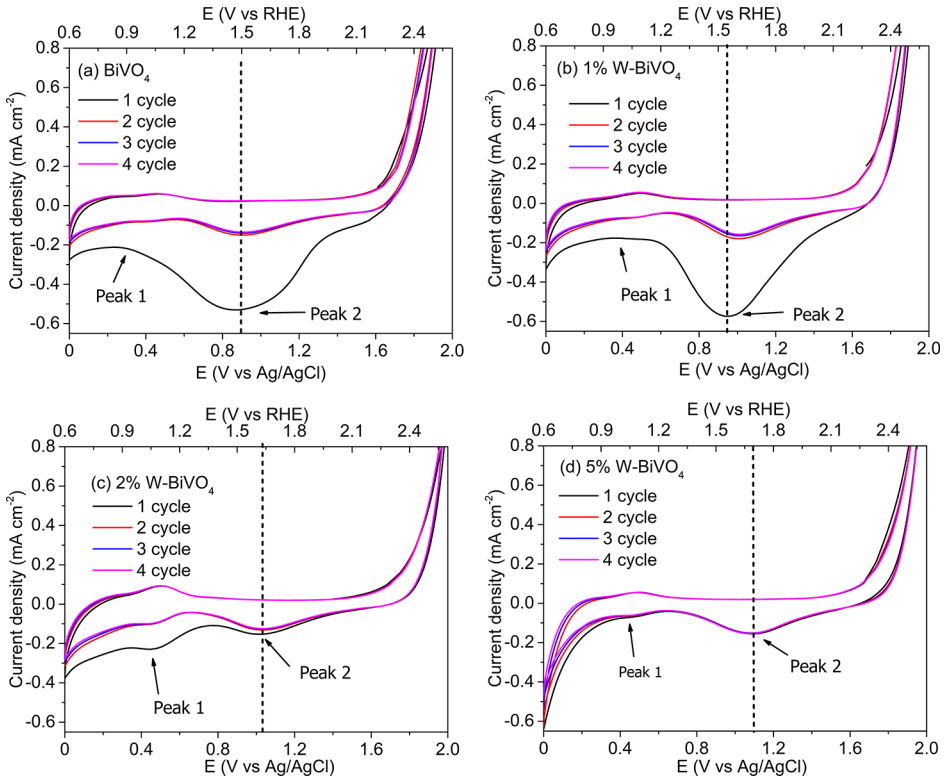

Figure 9. Cyclic voltammograms recorded in the dark at 2000 mV s^{-1} for four cycles immediately after holding the potential at 2 $V_{Ag/AgCl}$ for 120 s under illumination: (a) $BiVO_4$, (b) 1% W-$BiVO_4$, (c) 2% W-$BiVO_4$, (d) 5% W-$BiVO_4$.

illumination clearly display two cathodic peaks. The cathodic peak at around 1 V_{RHE} corresponds to the electron trapping process for the reduction of V^{5+} to V^{4+} in the bulk as discussed above. The cathodic peak at around 1.55 V_{RHE} in the dark agrees with the intrinsic surface reaction of VO_2^+/VO^{2+}, corresponding to the reductive reaction in eq 7.[46] Similar to the redox process of V^{4+}/V^{5+} in the bulk, the surface reaction of VO_2^+/VO^{2+} is also significantly favored under illumination, which can be attributed to another photoelectron trapping process (eq 8).

$$VO_2^+(\text{surface}) + 2H^+(aq) + e^-_{\text{inject}} \rightarrow VO^{2+}(\text{surface}) + H_2 \quad (7)$$

$$\text{Trapping: } VO_2^+(\text{surface}) + 2H^+(aq) + e^-_{\text{photo}} \rightarrow VO^{2+}(\text{surface}) + H_2 \quad (8)$$

Note that the VO_2^+/VO^{2+} surface reaction under illumination is an intrinsic irreversible reaction, indicating that not only is the charge transfer from the traps slow but also the detrapping process.[31] Interestingly, the surface reaction of VO_2^+/VO^{2+} seems to become reversible for 1% W-$BiVO_4$ in the dark (Figure S12), possibly because the introduction of an inadaptable amount of W atoms changes the surface properties of $BiVO_4$, leading to a change in the local structure. When the detrapping process is slow, the charges would be accumulated in the traps and then increase recombination as described by eq 9 and Figure S15.

$$VO_2^+(\text{surface}) + 2H^+(aq) \xleftrightarrow{(e^-_{\text{photo}}+h_{\text{trap}})_{\text{recombination}}} VO^{2+}(\text{surface}) \quad (9)$$

As a consequence, we attribute r-SS to the formation of trap states by the electron trapping process (eq 8) on the surface. Although the peak maximum potential is higher than the water oxidation potential (1.23 V_{RHE}), the potential range of this state covers the water oxidation during illumination (Figure 8). Therefore, one of the main causes of the low PEC performance for the $BiVO_4$ electrode might be the presence of r-SS.

3.5. Improvement of i-SS and Passivation of r-SS by W Doping. The previous observations indicate that i-SS and r-SS are attributed to the reduction of V^{5+} species in the bulk and on the surface, respectively, under illumination. Reasonably, it is important to observe the reductive behavior of V^{5+} species on the pristine/W-doped $BiVO_4$ electrodes to determine the effect of W-doping on the i-SS and r-SS. A typical CV measurement reported by Hamann et al. was carried out in the dark for the pristine/W-doped $BiVO_4$ electrodes (Figure 9).[23] For this purpose, the electrodes were held at 2 V vs Ag/AgCl ($V_{Ag/AgCl}$) under illumination for 120 s to fully oxidize the SS.[23,24,26] The following cathodic scan in the dark shows cathodic peaks corresponding to the reduction of SS, which is equivalent to recombination of surface trapped holes with conduction band electrons.[25] The resulting curves clearly display two cathodic peaks at around 1.0 V_{RHE} (peak 1) and 1.55 V_{RHE} (peak 2) in the first cycle. These peaks decrease significantly in the second cycle due to the transient nature of the oxidized states.[25,26] On the one hand, peak 1 is consistent with the electron trapping process for the reduction of V^{5+} to V^{4+} in bulk. This is equivalent to filling the i-SS, which is associated with water oxidation according to the above description. The reversible redox process of V^{4+}/V^{5+} can be observed both under dark and illumination conditions, indicating they belong to intrinsic surface states.[31] The chopped LSVs for all electrodes in Figure S16 show negative current transients only in the low applied

DOI: 10.1021/acscatal.7b04277
ACS Catal. XXXX, XXX, XXX−XXX

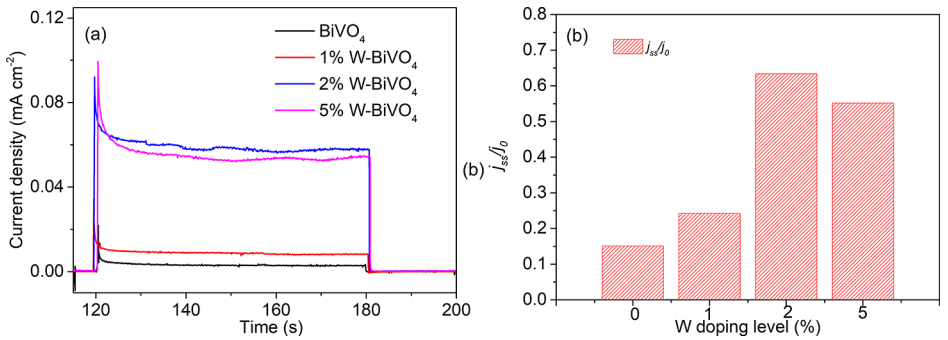

Figure 10. Chopped chronoamperometry plot (a) and plots of the photocurrent ratios j_{ss}/j_0 (b) of $BiVO_4$, 1% W-$BiVO_4$, 2% W-$BiVO_4$, and 5% W-$BiVO_4$ electrodes under back side illumination at 1.23 V_{RHE}.

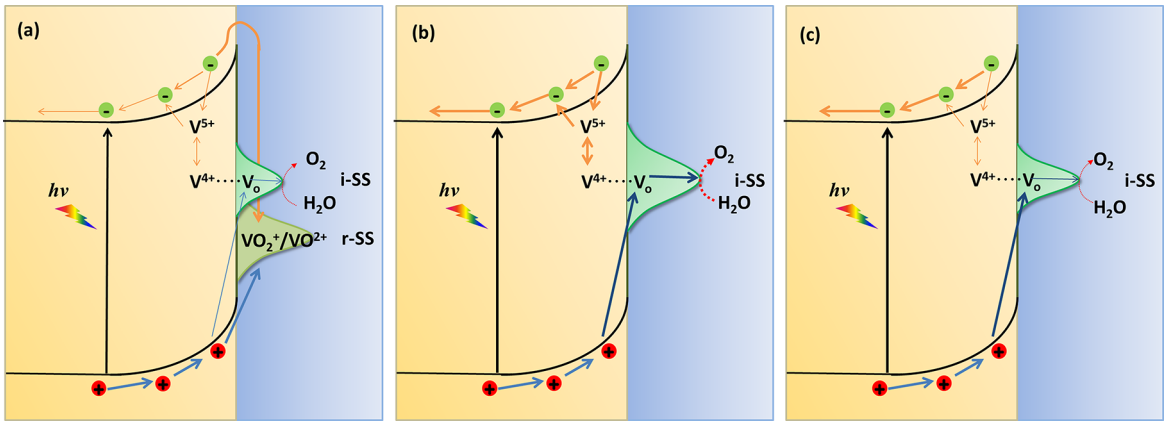

Figure 11. Schematic illustration of the proposed mechanism as a function of the W doping level: low (a), middle (b), and high (c; the thicker the arrow, the faster the process).

potential region (about 0.6−0.8 V_{RHE}). These current transients observed upon turning the light off represent the accumulated holes reacting with free electrons in the conduction band.[47] No negative current transients at higher potential can be explained by the fact that i-SS is activated, promoting charge transfer at SEI, similar to the IrO_x catalyst for the hematite electrode.[31] On the other hand, peak 2 corresponds to the electron trapping process for the surface reductive reaction of VO_2^+ to VO^{2+}, which is assigned to r-SS. In fact, this reaction is intrinsic in the $BiVO_4$ electrode as well as the reduction of V^{5+} to V^{4+} in the bulk, since the cathodic peaks are present in all cycles of the CV.

As can be seen, the peak 2 intensity clearly decreases with increasing the content of the W dopant, and the potentials shift to a more anodic potential (Figure 9). According to the area of peak 2, it can be inferred that the concentrations of r-SS for the photoanodes follow the order 5% W-$BiVO_4$ < 2% W-$BiVO_4$ < 1% W-$BiVO_4$ < $BiVO_4$ electrodes. $BiVO_4$ and 1% W-$BiVO_4$ suffer a huge number of surface recombinations, thereby lowering PEC performance (Figure S3). Interestingly, peak 1 is high in $BiVO_4$ and 1% W-$BiVO_4$, suggesting they also present high concentrations of i-SS after the pretreatment to fully oxidize the SS. This is in agreement with the surface recombination limitation of $BiVO_4$ reported by van der Krol et al., rather than the charge transfer.[48] The reason why $BiVO_4$ and 1% W-$BiVO_4$ show low SS (in Figure 5b) without fully oxidized SS is that most of photogenerated electrons are trapped for r-SS so that there are less for i-SS. Therefore, $BiVO_4$ and 1% W-$BiVO_4$ present low charge transfer efficiency at i-SS (Figure 5a). The r-SS is passivated remarkably in 2% and 5% W-$BiVO_4$ electrodes. The intensity of peak 1 for 5% W-$BiVO_4$ is significantly lower than that of 2% W-$BiVO_4$. Clearly, 2% W-$BiVO_4$ shows slightly higher r-SS than 5% W-$BiVO_4$, but 2% W-$BiVO_4$ has a quite larger i-SS than 5% W-$BiVO_4$, in line with the results in Figure 5b. This suggests that the PEC performance mainly depends on i-SS related to the bulk properties when the surface recombination is suppressed. The Bode plots analysis can further support this suggestion. Figure S17 displays the Bode plots for all photoanodes at three selected potentials (0.7, 1.0, and 1.3 V_{RHE}) under illumination. The higher the phase value, the more capacitive is the behavior of the system, reflecting the accumulation of charge at a certain interface.[38] The low frequency peak at around 200 mHz is related to the capacitance at SEI. It disappears in 2% and 5% W-$BiVO_4$ at 1.0 and 1.3 V_{RHE}, suggesting the charge transfer at SEI is fast and the PEC water oxidation is limited mainly by the intrinsic properties of the semiconductor bulk.[38] The electron−hole recombination processes are further studied by the photocurrent−time transient measurements at 1.23 V_{RHE} (Figure 10). The steady state photocurrent reached after a certain period of illumination (j_{ss}) of all electrodes follows the order $BiVO_4$ < 1% W-$BiVO_4$ < 5% W-$BiVO_4$ < 2% W-$BiVO_4$, in line with the LSV measurements. Figure 10b shows the ratio between j_{ss} and the initial photocurrent spike, when the light is switched on (j_0), obtained from Figure 10a. This ratio j_{ss}/j_0 can be explained in terms of electron back reaction that is superimposed to the anodic photocurrent.[3] For the back reaction, it can be considered that the electrons promoted to the conduction band from the valence band are (1) recombined with hole in bulk and (2) trapped at surface states at SEI and

DOI: 10.1021/acscatal.7b04277
ACS Catal. XXXX, XXX, XXX−XXX

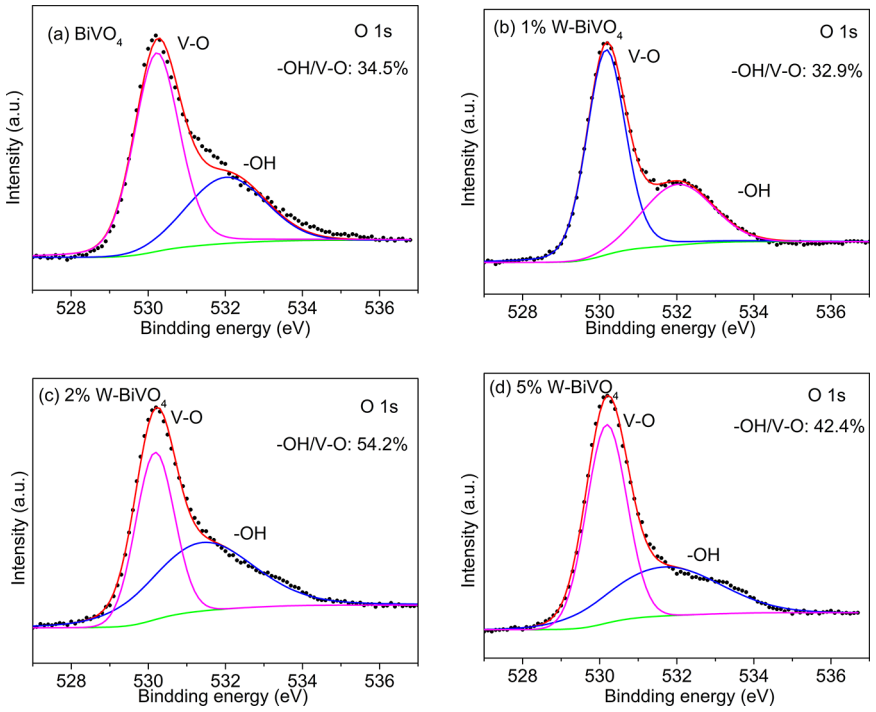

Figure 12. High resolution XPS spectra in the O 1s region of (a) $BiVO_4$, (b) 1% W-$BiVO_4$, (c) 2% W-$BiVO_4$, and (d) 5% W-$BiVO_4$. The inset number is the peak area ratio of −OH/V−O.

then recombined with accumulated holes. The pristine $BiVO_4$ and 1% W-$BiVO_4$ show low values of j_{ss}/j_0, implying they suffer a fast electron back reaction. The ratio of j_{ss}/j_0 reaches its maximum at a 2% W doping level but decreases at a 5% W doping level. The electron back reaction for surface recombination in 5% W-$BiVO_4$ is very slow due to its low concentration of r-SS. However, the lower N_d of 5% W-$BiVO_4$ would result in a fast electron back reaction for recombination in bulk. It can be further confirmed that the bulk properties would dominate the PEC performance when the surface recombination is suppressed.

On the basis of the above discussion, a model is depicted in Figure 11 to illustrate the proposed mechanism as a function of the W doping level (low, middle, and high). Upon illumination, a photoelectron trapping process can be generated in two ways: trapping for the reversible redox process of V^{5+}/V^{4+} in semiconductor bulk and irreversible surface reduction of VO_2^+ to VO^{2+} on the surface. The former does not raise recombination benefitting from its fast detrapping process, and the intermediate V^{4+} can introduce V_o, which can adsorb oxy/hydroxyl species on the surface, forming i-SS. Otherwise, the latter produces r-SS due to the slow detrapping process. Meanwhile, substitution of V^{5+} by W^{6+} can produce more V^{4+} and increase the N_d for the host lattice, resulting in a suppression of the electron bulk and surface trapping.

For a low W doping level (Figure 11a), due to the low N_d, the charge separation is not efficient, and back-reaction processes are fast for the photogenerated electron created close to the surface. Thus, the electron is easily trapped by VO_2^+, generating a large concentration of r-SS that results in a fast hole transfer for surface recombination. As a consequence, the hole transfer to i-SS for water oxidation is slow, leading to low PEC performance. At a middle W doping level (Figure 11b), with higher film conductivity and more substitutional W atoms on the surface, the surface electron trapping process is suppressed so that the r-SS is passivated. Therefore, the electron trapping process in the bulk is favored, producing a high concentration of i-SS, which improves the hole transfer for water oxidation. Finally, for a higher W doping level (Figure 11c), not only surface reductive reaction of VO_2^+/VO^{2+} but also the redox process of V^{4+}/V^{5+} in the bulk are weakened, so there are no r-SS's and a low concentration of i-SS. The proposed mechanism can be further confirmed by XPS analysis. Figure 12 shows the high-resolution XPS spectra in the O 1s region for all photoanodes. The peak can be assigned to surface lattice oxygen (V−O) at around 530 eV and surface adsorbed oxygen (−OH) at around 532 eV.[49,50] The peak area ratios of −OH/V−O in $BiVO_4$ and 1% W-$BiVO_4$ are 34.5 and 32.9%, respectively. The ratio increases to 54.2% in 2% W-$BiVO_4$ and then decreases again in 5% W-$BiVO_4$ (42.4%). The enhancement of −OH presence reflects an increased concentration of surface V_o, implying a high amount of i-SS. The change trend in −OH species concentration is in agreement with the i-SS behavior in the electrodes with increasing W doping level.

CONCLUSIONS

The i-SS and r-SS are observed on the pristine and W-doped $BiVO_4$ photoanodes fabricated by electrospinning for PEC water oxidation. The reversible redox process of V^{4+}/V^{5+} in bulk can induce V_o by an electron trapping process, which can adsorb oxy/hydroxyl species on the surface to form i-SS, while the irreversible surface reaction of VO_2^+/VO^{2+} generated at higher potential can trap the photogenerated electron to form r-SS. W-doping is confirmed to modify the bulk and surface properties of the $BiVO_4$ electrode by suppressing the electron trapping processes in bulk and on the surface. The optimum intermediate W-doping level (2%) is suggested to remove the r-SS but preserve the i-SS. As a result of that, 2% W-$BiVO_4$ shows a remarkable photocurrent increase with respect to the pristine $BiVO_4$ at 1.23 V_{RHE}, in line with impedance measurements that

DOI: 10.1021/acscatal.7b04277
ACS Catal. XXXX, XXX, XXX−XXX

show the lowest total charge transfer resistance and the highest concentration of i-SS. It is suggested that a high PEC performance requires not only a large total N_{SS}/N_d ratio but also numerous total N_{SS} and N_d to give both good conductivity and enough surface reactive sites. This paper provides a further understanding of the fundamentals for the enhancement of PEC performance and would help to design photoanodes for solar-driven water oxidation or wastewater treatment.

■ ASSOCIATED CONTENT

Supporting Information

The Supporting Information is available free of charge on the ACS Publications website at DOI: 10.1021/acscatal.7b04277.

XRD data, UV−vis, LSV data, equivalent circuits, additional CV curves, Nyquist plots, data of N_{SS} and N_d, Mott−Schottky plots, Bode plots, double-layer capacitance, and schemes to illustrate mechanism related to the SS (PDF)

■ AUTHOR INFORMATION

Corresponding Authors

*E-mail: wanghui@bjfu.edu.cn.

*E-mail: tandreu@irec.cat.

ORCID

Sebastián Murcia-López: 0000-0002-3703-041X

Hui Wang: 0000-0002-6299-4034

Teresa Andreu: 0000-0002-2804-4545

Author Contributions

The manuscript was written through contributions of all authors. All authors have given approval to the final version of the manuscript.

Notes

The authors declare no competing financial interest.

■ ACKNOWLEDGMENTS

The authors from IREC thank Generalitat de Catalunya for financial support through the CERCA Program, M2E (2014SGR1638), and XaRMAE. Q.S. acknowledges financial support from the China Scholarship Council through a Ph.D. scholarship (No. 201606510020). IREC also acknowledges support by the European Regional Development Funds (ERDF, FEDER) and by MINECO project ENE2016-80788-C5-5-R. S.M.-L. thanks MINECO for his Juan de la Cierva—Formación fellowship (FJCI-2014-19745), and European Union's Horizon 2020 and the Agency for Business Competitiveness of the Government of Catalonia for funding under the Marie Sklodowska-Curie grant agreement No. 712939 (TECNIOspring PLUS). H.W. and Q.S. are thankful for financial support from the Fundamental Research Funds for the Central Universities (No. 2016ZCQ03), Beijing Natural Science Foundation (No. 8172035). P.T. acknowledges the work performed in the framework of Universitat Autònoma de Barcelona Materials Science Ph.D. program.

■ REFERENCES

(1) Park, Y.; McDonald, K. J.; Choi, K. S. Progress in bismuth vanadate photoanodes for use in solar water oxidation. *Chem. Soc. Rev.* **2013**, *42*, 2321−2337.

(2) Ding, C. M.; Shi, J. Y.; Wang, Z. L.; Li, C. Photoelectrocatalytic Water Splitting: Significance of Cocatalysts, Electrolyte, and Interfaces. *ACS Catal.* **2017**, *7*, 675−688.

(3) Fàbrega, C.; Monllor-Satoca, D.; Ampudia, S.; Parra, A.; Andreu, T.; Morante, J. R. Tuning the Fermi Level and the Kinetics of Surface States of TiO_2 Nanorods by Means of Ammonia Treatments. *J. Phys. Chem. C* **2013**, *117*, 20517−20524.

(4) Murcia-López, S.; Fàbrega, C.; Monllor-Satoca, D.; Hernández-Alonso, M. D.; Penelas-Pérez, G.; Morata, A.; Morante, J. R.; Andreu, T. Tailoring Multilayered $BiVO_4$ Photoanodes by Pulsed Laser Deposition for Water Splitting. *ACS Appl. Mater. Interfaces* **2016**, *8*, 4076−4085.

(5) Monllor-Satoca, D.; Bärtsch, M.; Fàbrega, C.; Genç, A.; Reinhard, S.; Andreu, T.; Arbiol, J.; Niederberger, M.; Morante, J. R. What do you do, titanium? Insight into the role of titanium oxide as a water oxidation promoter in hematite-based photoanodes. *Energy Environ. Sci.* **2015**, *8*, 3242−3254.

(6) Tang, P. Y.; Xie, H. B.; Ros, C.; Han, L. J.; Biset-Peiró, M.; He, Y. M.; Kramer, W.; Rodríguez, A. P.; Saucedo, E.; Galán-Mascarós, J. R.; Andreu, T.; Morante, J. R.; Arbiol, J. Enhanced photoelectrochemical water splitting of hematite multilayer nanowire photoanodes by tuning the surface state via bottom-up interfacial engineering. *Energy Environ. Sci.* **2017**, *10*, 2124−2136.

(7) Yu, F. S.; Li, F.; Yao, T. T.; Du, J.; Liang, Y. Q.; Wang, Y.; Han, H. X.; Sun, L. C. Fabrication and Kinetic Study of a Ferrihydrite-Modified $BiVO_4$ Photoanode. *ACS Catal.* **2017**, *7*, 1868−1874.

(8) Murcia-López, S.; Bacariza, M. C.; Villa, K.; Lopes, J. M.; Henriques, C.; Morante, J. R.; Andreu, T. Controlled Photocatalytic Oxidation of Methane to Methanol through Surface Modification of Beta Zeolites. *ACS Catal.* **2017**, *7*, 2878−2885.

(9) Trześniewski, B. J.; Digdaya, I. A.; Nagaki, T.; Ravishankar, S.; Herraiz-Cardona, I.; Vermaas, D. A.; Longo, A.; Gimenez, S.; Smith, W. A. Near-complete suppression of surface losses and total internal quantum efficiency in $BiVO_4$ photoanodes. *Energy Environ. Sci.* **2017**, *10*, 1517−1529.

(10) Zhang, K. F.; Liu, Y. X.; Deng, J. G.; Xie, S. H.; Lin, H. X.; Zhao, X. T.; Yang, J.; Han, Z.; Dai, H. X. Fe_2O_3/3DOM $BiVO_4$: High-performance photocatalysts for the visible light-driven degradation of 4-nitrophenol. *Appl. Catal., B* **2017**, *202*, 569−579.

(11) Thalluri, S. M.; Hernández, S.; Bensaid, S.; Saracco, G.; Russo, N. Green-synthesized W- and Mo-doped $BiVO_4$ oriented along the 040 facet with enhanced activity for the sun-driven water oxidation. *Appl. Catal., B* **2016**, *180*, 630−636.

(12) Antony, R. P.; Bassi, P. S.; Abdi, F. F.; Chiam, S. Y.; Ren, Y.; Barber, J.; Loo, J. S. C.; Wong, L. H. Electrospun Mo-$BiVO_4$ for Efficient Photoelectrochemical Water Oxidation: Direct Evidence of Improved Hole Diffusion Length and Charge separation. *Electrochim. Acta* **2016**, *211*, 173−182.

(13) Choi, J.; Sudhagar, P.; Kim, J. H.; Kwon, J.; Kim, J.; Terashima, C.; Fujishima, A.; Song, T.; Paik, U. WO_3/W:$BiVO_4$/$BiVO_4$ graded photoabsorber electrode for enhanced photoelectrocatalytic solar light driven water oxidation. *Phys. Chem. Chem. Phys.* **2017**, *19*, 4648−4655.

(14) Gutkowski, R.; Khare, C.; Conzuelo, F.; Kayran, Y. U.; Ludwig, A.; Schuhmann, W. Unraveling compositional effects on the light-induced oxygen evolution in Bi(V−Mo−X)O_4 material libraries. *Energy Environ. Sci.* **2017**, *10*, 1213−1221.

(15) Berglund, S. P.; Rettie, A. J. E.; Hoang, S.; Mullins, C. B. Incorporation of Mo and W into nanostructured $BiVO_4$ films for efficient photoelectrochemical water oxidation. *Phys. Chem. Chem. Phys.* **2012**, *14*, 7065−7075.

(16) Park, H. S.; Kweon, K. E.; Ye, H.; Paek, E.; Hwang, G. S.; Bard, A. J. Factors in the Metal Doping of $BiVO_4$ for Improved Photoelectrocatalytic Activity as Studied by Scanning Electrochemical Microscopy and First-Principles Density-Functional Calculation. *J. Phys. Chem. C* **2011**, *115*, 17870−17879.

(17) Yin, W. J.; Wei, S. H.; Al-Jassim, M. M.; Turner, J.; Yan, Y. F. Doping properties of monoclinic $BiVO_4$ studied by first-principles density-functional theory. *Phys. Rev. B: Condens. Matter Mater. Phys.* **2011**, *83*, 155102.

(18) Zhang, B.; Zhang, H. P.; Wang, Z. Y.; Zhang, X. Y.; Qin, X. Y.; Dai, Y.; Liu, Y. Y.; Wang, P.; Li, Y. J.; Huang, B. B. Enhancing the

DOI: 10.1021/acscatal.7b04277
ACS Catal. XXXX, XXX, XXX−XXX

Photocatalytic Activity of $BiVO_4$ for Oxygen Evolution by Ce Doping: Ce^{3+} Ions as Hole Traps. *Appl. Catal., B* **2017**, *211*, 258−265.
(19) Pattengale, B.; Ludwig, J.; Huang, J. Atomic Insight into the W-Doping Effect on Carrier Dynamics and Photoelectrochemical Properties of $BiVO_4$ Photoanodes. *J. Phys. Chem. C* **2016**, *120*, 1421−1427.
(20) Jo, W. J.; Jang, J. W.; Kong, K. J.; Kang, H. J.; Kim, J. Y.; Jun, H.; Parmar, K. P. S.; Lee, J. S. Phosphate doping into monoclinic $BiVO_4$ for enhanced photoelectrochemical water oxidation activity. *Angew. Chem., Int. Ed.* **2012**, *51*, 3147−3151.
(21) Abdi, F. F.; Savenije, T. J.; May, M. M.; Dam, B.; van de Krol, R. The Origin of Slow Carrier Transport in BiVO4 Thin Film Photoanodes: A Time-Resolved Microwave Conductivity Study. *J. Phys. Chem. Lett.* **2013**, *4*, 2752−2757.
(22) Wang, Z. L.; Fan, F. T.; Wang, S. Y.; Ding, C. M.; Zhao, Y. L.; Li, C. Bridging surface states and current−potential response over hematite-based photoelectrochemical water oxidation. *RSC Adv.* **2016**, *6*, 85582.
(23) Klahr, B.; Gimenez, S.; Fabregat-Santiago, F.; Bisquert, J.; Hamann, T. W. Electrochemical and photoelectrochemical investigation of water oxidation with hematite electrodes. *Energy Environ. Sci.* **2012**, *5*, 7626−7636.
(24) Zandi, O.; Hamann, T. W. Determination of photoelectrochemical water oxidation intermediates on haematite electrode surfaces using operando infrared spectroscopy. *Nat. Chem.* **2016**, *8*, 778−783.
(25) Gao, Y.; Hamann, T. W. Elucidation of $CuWO_4$ Surface States During Photoelectrochemical Water Oxidation. *J. Phys. Chem. Lett.* **2017**, *8*, 2700−2704.
(26) Zandi, O.; Hamann, T. W. Enhanced Water Splitting Efficiency Through Selective Surface State Removal. *J. Phys. Chem. Lett.* **2014**, *5*, 1522−1526.
(27) Le Formal, F.; Tétreault, N.; Cornuz, M.; Moehl, T.; Grätzel, M.; Sivula, K. Passivating surface states on water splitting hematite photoanodes with alumina overlayers. *Chem. Sci.* **2011**, *2*, 737−743.
(28) Cho, S. K.; Park, H. S.; Lee, H. C.; Nam, K. M.; Bard, A. J. Metal Doping of $BiVO_4$ by Composite Electrodeposition with Improved Photoelectrochemical Water Oxidation. *J. Phys. Chem. C* **2013**, *117*, 23048−23056.
(29) Jovic, V.; Rettie, A. J. E.; Singh, V. R.; Zhou, J. S.; Lamoureux, B.; Mullins, C. B.; Bluhm, H.; Laverock, J.; Smith, K. E. A soft X-ray spectroscopic perspective of electron localization and transport in tungsten doped bismuth vanadate single crystals. *Phys. Chem. Chem. Phys.* **2016**, *18*, 31958−31965.
(30) Pinaud, B. A.; Vesborg, P. C. K.; Jaramillo, T. F. Effect of Film Morphology and Thickness on Charge Transport in Ta_3N_5/Ta Photoanodes for Solar Water Splitting. *J. Phys. Chem. C* **2012**, *116*, 15918−15924.
(31) Trasatti, S.; Petrii, O. A. Real surface area measurements in electrochemistry. *J. Electroanal. Chem.* **1992**, *327*, 353−376.
(32) Ramsundar, R. M.; Debgupta, J.; Pillai, V. K.; Joy, P. A. Electrochemical Synthesis of Spinel Type $ZnCo_2O_4$ Electrodes for Use as Oxygen Evolution Reaction Catalysts. *Electrocatalysis* **2015**, *6*, 331−340.
(33) McCrory, C. C. L.; Jung, S.; Peters, J. C.; Jaramillo, T. F. Benchmarking Heterogeneous Electrocatalysts for the Oxygen Evolution Reaction. *J. Am. Chem. Soc.* **2013**, *135*, 16977−16987.
(34) Zhang, Y.; Wang, D.; Zhang, X. T.; Chen, Y.; Kong, L. N.; Chen, P.; Wang, Y. L.; Wang, C. H.; Wang, L. L.; Liu, Y. C. Enhanced photoelectrochemical performance of nanoporous $BiVO_4$ photoanode by combining surface deposited cobalt-phosphate with hydrogenation treatment. *Electrochim. Acta* **2016**, *195*, 51−58.
(35) Bertoluzzi, L.; Badia-Bou, L.; Fabregat-Santiago, F.; Gimenez, S.; Bisquert, J. Interpretation of Cyclic Voltammetry Measurements of Thin Semiconductor Films for Solar Fuel Applications. *J. Phys. Chem. Lett.* **2013**, *4*, 1334−1339.
(36) Gromboni, M. F.; Coelho, D.; Mascaro, L. H.; Pockett, A.; Marken, F. Enhancing activity in a nanostructured $BiVO_4$ photoanode with a coating of microporous Al_2O_3. *Appl. Catal., B* **2017**, *200*, 133−140.
(37) Klahr, B.; Gimenez, S.; Fabregat-Santiago, F.; Hamann, T.; Bisquert, J. Water Oxidation at Hematite Photoelectrodes: The Role of Surface States. *J. Am. Chem. Soc.* **2012**, *134*, 4294−4302.
(38) Malara, F.; Minguzzi, A.; Marelli, M.; Morandi, S.; Psaro, R.; Dal Santo, V.; Naldoni, A. α-Fe_2O_3/NiOOH: An Effective Heterostructure for Photoelectrochemical Water Oxidation. *ACS Catal.* **2015**, *5*, 5292−5300.
(39) Hajibabaei, H.; Schon, A. R.; Hamann, T. W. Interface Control of Photoelectrochemical Water Oxidation Performance with $Ni_{1-x}Fe_xO_y$ Modified Hematite Photoanodes. *Chem. Mater.* **2017**, *29*, 6674−6683.
(40) Cummings, C. Y.; Marken, F.; Peter, L. M.; Tahir, A. A.; Wijayantha, K. G. U. Kinetics and mechanism of light-driven oxygen evolution at thin film α-Fe_2O_3 electrodes. *Chem. Commun.* **2012**, *48*, 2027−2029.
(41) Shi, Q.; Wang, H.; Liu, S. L.; Pang, L.; Bian, Z. Y. *Electrochim. Acta* **2015**, *178*, 92−100.
(42) Song, X. Z.; Xu, D. D.; Shi, Q.; Wang, F.; Wang, H.; Bian, Z. Y. Abundant Size-Controlled Cu-Ni(Fe) Alloy Nanoparticles Decorated Reduced Graphene with Enhanced Electrocatalytic Activities for Chloramphenicol. *J. Electrochem. Soc.* **2017**, *164*, H779−H787.
(43) Song, X. Z.; Shi, Q.; Wang, H.; Liu, S. L.; Tai, C.; Bian, Z. Y. Preparation of Pd-Fe/graphene catalysts by photocatalytic reduction with enhanced electrochemical oxidation-reduction properties for chlorophenols. *Appl. Catal., B* **2017**, *203*, 442−451.
(44) Zhang, Y. Y.; Guo, Y. P.; Duan, H. N.; Li, H.; Sun, C. Y.; Liu, H. Z. Facile synthesis of V^{4+} self-doped, [010] oriented $BiVO_4$ nanorods with highly efficient visible light-induced photocatalytic activity. *Phys. Chem. Chem. Phys.* **2014**, *16*, 24519−24526.
(45) Hu, J.; Zhao, X.; Chen, W.; Su, H. B.; Chen, Z. Theoretical Insight into the Mechanism of Photoelectrochemical Oxygen Evolution Reaction on $BiVO_4$ Anode with Oxygen Vacancy. *J. Phys. Chem. C* **2017**, *121*, 18702−1879.
(46) Jin, J. T.; Fu, X. G.; Liu, Q.; Liu, Y. R.; Wei, Z. Y.; Niu, K. X.; Zhang, J. Y. Identifying the Active Site in Nitrogen-Doped Graphene for the VO_{2+}/VO_2^+ Redox Reaction. *ACS Nano* **2013**, *7*, 4764−4773.
(47) Abdi, F. F.; van de Krol, R. Nature and Light Dependence of Bulk Recombination in Co-Pi-Catalyzed $BiVO_4$ Photoanodes. *J. Phys. Chem. C* **2012**, *116*, 9398−9404.
(48) Zachäus, C.; Abdi, F. F.; Peter, L. M.; van de Krol, R. Photocurrent of $BiVO_4$ is limited by surface recombination, not surface catalysis. *Chem. Sci.* **2017**, *8*, 3712−3719.
(49) Zhu, M. Y.; Liu, Q.; Chen, W.; Yin, Y. Y.; Ge, L.; Li, H. N.; Wang, K. Boosting the Visible-Light Photoactivity of BiOCl/$BiVO_4$/N-GQD Ternary Heterojunctions Based on Internal Z-Scheme Charge Transfer of N-GQDs: Simultaneous Band Gap Narrowing and Carrier Lifetime Prolonging. *ACS Appl. Mater. Interfaces* **2017**, *9*, 38832−38841.
(50) Shi, Q.; Song, X. Z.; Wang, H.; Bian, Z. Y. Enriched Photoelectrochemical Performance of Phosphate Doped $BiVO_4$ Photoelectrode by Coupling FeOOH and rGO. *J. Electrochem. Soc.* **2018**, *165*, H3018−H3027.

DOI: 10.1021/acscatal.7b04277
ACS Catal. XXXX, XXX, XXX−XXX